

FIDO science payload simulating the Athena Payload

Albert F. C. Haldemann,¹ Eric T. Baumgartner,¹ Gregory H. Bearman,¹
 Diana L. Blaney,¹ David I. Brown,¹ Benjamin P. Dolgin,¹ Leonard I. Dorsky,¹
 Terrance L. Huntsberger,¹ Alexander Ksendzov,¹ J. Colin Mahoney,¹
 Mark J. McKelvey,¹ Betina E. Pavri,¹ Gabriel A. Post,¹ Eldred F. Tubbs,¹
 Raymond E. Arvidson,² Nathaniel O. Snider,² Steven W. Squyres,³ Stephen Gorevan,⁴
 Göstar Klingelhöfer,⁵ Bodo Bernhardt,⁵ and Ralf Gellert⁵

Received 3 October 2001; revised 20 February 2002; accepted 19 April 2002; published 4 October 2002.

[1] The Jet Propulsion Laboratory's Field Integrated Development and Operations rover (FIDO) emulates and tests operational rover capabilities for advanced Mars rover missions, such as those originally planned for the Mars Surveyor 2001 Rover and currently planned for the Athena Payload on the Mars Exploration Rovers scheduled for launch in 2003. This paper describes FIDO's science instrument payload, which is fully integrated with rover hardware and software. Remote science teams visualize instrument suite data and generate FIDO commands using the Web Interface for Telescience. FIDO's instrument suite has been used in terrestrial laboratory and field tests to simulate Mars operations, to train Mars scientists, and to improve Mars rover mission science operations protocols. The payload includes a deck-mounted, stowable mast that is deployed for acquisition of stereo imaging and spectral reflectance data. The mast head houses Pancam, Navcam (the navigation camera stereo pair), and the Infrared Point Spectrometer (IPS). Pancam is a three-band, false-color infrared (0.65, 0.74, 0.855 μm) stereo imaging system. The three wavelengths were chosen to yield information on the ferric nature of observed minerals. IPS acquires spectral radiance information over the wavelengths from 1.3 to 2.5 μm (spectral resolution $\sim 13 \text{ cm}^{-1}$). A 4-degree-of-freedom arm is included on the front of FIDO. The arm end effector is the mounting point for a Color Microscopic Imager and an ^{57}Fe Mössbauer Spectrometer. FIDO also carries a MiniCorer, which is an Athena prototype rock drill that can acquire 0.5-cm-diameter by up to 1.7-cm-long cores. *INDEX TERMS:* 5494 Planetology: Solid Surface Planets: Instruments and techniques; 5464 Planetology: Solid Surface Planets: Remote sensing; 6297 Planetology: Solar System Objects: Instruments and techniques; 6225 Planetology: Solar System Objects: Mars; *KEYWORDS:* Rover, mobility, in situ instruments, integrated payload, FIDO, Mars

Citation: Haldemann, A. F. C., et al., FIDO science payload simulating the Athena Payload, *J. Geophys. Res.*, 107(E11), 8006, doi:10.1029/2001JE001738, 2002.

1. Introduction

[2] The Jet Propulsion Laboratory's (JPL) Field Integrated Development and Operations rover (FIDO) [Schenker *et al.*, 2001; Arvidson *et al.*, 2002] deploys an integrated instrument suite to test rover capabilities in conjunction with operations concepts for advanced Mars rover missions, such

as those originally planned for the Mars Surveyor 2001 Lander and currently planned for the Athena Payload on the Mars Exploration Rovers. FIDO also tests capabilities required for future Mars Sample Return missions using rovers for sample acquisition. FIDO and its integrated instrument suite are operated by a remote science team using the Web Interface for Telescience (WITS) for data visualization and command sequence generation [Backes *et al.*, 1997; Backes and Norris, 2001]. Verified command sequences are sent to FIDO, which then autonomously carries out its charge.

[3] FIDO is a 75-kg rover that can travel hundreds of meters per day using onboard stereo image analysis software for obstacle avoidance. The rover payload includes cameras and sensors that accomplish rover mobility tasks and science objectives. Some of the instruments are located on a deployable mast, while others reside at the end of a robotic arm (Figure 1). This paper describes

¹Jet Propulsion Laboratory, California Institute of Technology, Pasadena, California, USA.

²Department of Earth and Planetary Sciences, Washington University, St. Louis, Missouri, USA.

³Center for Radiophysics and Space Research, Cornell University, Ithaca, New York, USA.

⁴Honeybee Robotics Inc., New York, New York, USA.

⁵Institute for Inorganic and Analytical Chemistry, Johannes Gutenberg University Mainz, Mainz, Germany.

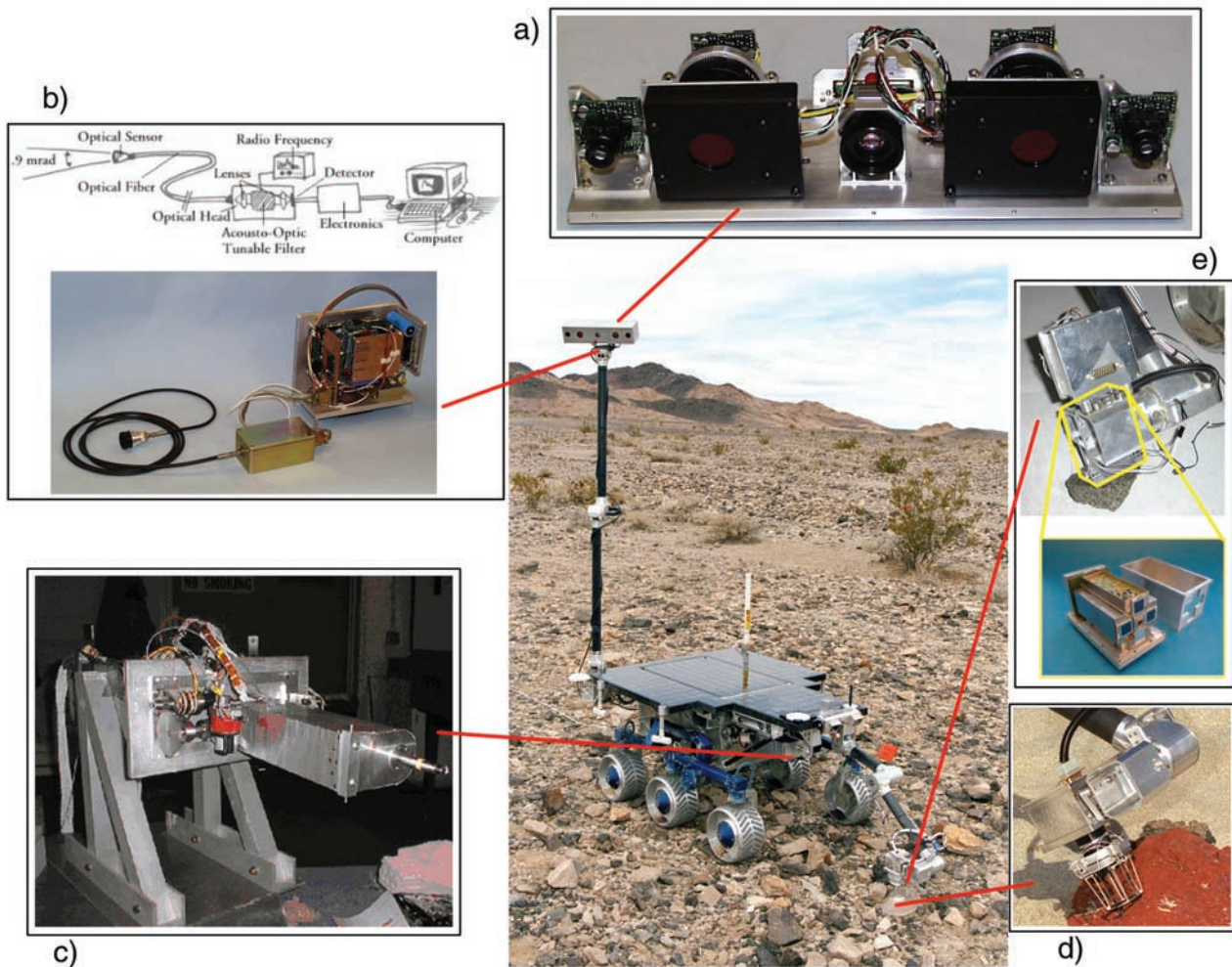


Figure 1. FIDO (center) during field tests and instruments. (a) Mast head assembly used during the 1999 field testing. The cameras on either end form the navigation camera stereo pair (Navcam). The two Panoramic Camera (Pancam) stereo pair cameras (located behind the thin black boxes containing the liquid crystal tunable filter (LCTF)) are off-the-shelf black-and-white CCD cameras. Camera 1 and filter 1 are on the right, and camera 2 and filter 2 are on the left as viewed looking out from FIDO. The fifth eye in the middle is the $f/3$ Infrared Point Spectrometer (IPS) foreoptics. (b) IPS schematic and IPS hardware with $f/3$ foreoptics. The computer in the diagram represents either a bench-top PC or the PC board inside FIDO. (c) MiniCorer on a test stand, which emulates variable rover stiffness, weight, deadband, and backlash. (d) Microscopic Imager (MI). (e) MIMOS II Mössbauer Spectrometer, deployed touching the rock and partially obscured by the wrist turret. The box with the reflective panel located above the wrist is the Microscopic Imager viewed from the rear. Close-up of Mössbauer Spectrometer with U.S. \$0.25 coin for scale.

FIDO's science instrument payload. Section 2 is a discussion of the rationale for developing FIDO as a first-order Athena Payload emulation. We enumerate the FIDO science instrument requirements and distinguish between the science payload and those instruments that enable roving. Sections 3 and 4 are descriptions of the two mast-mounted science instruments, the Panoramic Camera (Pancam) and the Infrared Point Spectrometer (IPS). Sections 5 and 6 contain descriptions of the two science instruments mounted to date on FIDO's robotic arm, and section 7 is a description FIDO's MiniCorer drilling system. Each instrument presentation includes (1) a technical description of the instrument and (2) a description of instrument

testing results, calibration, noise levels, and laboratory and field performance. Outdoor test results include some from the JPL Mars Yard. The JPL Mars Yard consists of some 400 m² of basaltic cobble- and boulder-strewn beach sand and red clay used for rover testing. As appropriate, the instrument sections also have a brief summary of operational use during 1999 and 2000 field testing and lessons learned from those tests. Results from the field tests are summarized by *Arvidson et al.* [2002], with details given by *Jolliff et al.* [2002] and *Moersch et al.* [2002]. Section 8 describes the integration of the instruments with the FIDO rover hardware and software and with each other via integrated operations to imple-

Table 1. Rover Science Payloads

Capability	Mission		
	Mars Surveyor 2001 Rover	MER ^a Mission	FIDO
High-resolution, color, stereo panoramic imaging Midinfrared spectrometry	Pancam	<i>Remote Sensing</i> ^b Pancam 15 filters 0.4–1.1 μm	Pancam 3 filters 650–855 nm
	MiniTES ^c	MiniTES	IPS ^d
Elemental chemical analysis Analysis of iron-bearing minerals Precise mineralogical identifications Close-up, fine-scale (30 $\mu\text{m}/\text{pixel}$) imaging Rock surface preparation	<i>In Situ Analysis</i> ^e		
	APXS ^f	APXS	none
	Mössbauer Spectrometer	Mössbauer Spectrometer	Mössbauer Spectrometer
	Raman Spectrometer	none	Raman Spectrometer ^g
	Microscopic Imager	Microscopic Imager	Microscopic Imager
Rock coring and soil sampling	(MiniCorer)	RAT ^h	Arm-mounted brush or hand-held abrasion tool MiniCorer ⁱ

^aMER, Mars Exploration Rover.

^bRemote-sensing capability instruments are mounted on masts in all cases.

^cMiniTES, MiniThermal Emission Spectrometer, operating in the mid-IR.

^dIPS, Infrared Point Spectrometer, operating in the near-IR.

^eIn situ analysis capability instruments are all mounted on some form of deployment device to enable direct access to soils or rocks at or near ground level.

^fAPXS, Alpha Proton X-ray Spectrometer.

^gOriginally planned, not yet implemented on board. Capability is partially implemented during field trials by laboratory testing of hand samples.

^hRAT, Rock Abrasion Tool.

ⁱFIDO MiniCorer only for rock coring.

ment Mars operations scenarios, as well as the more general lessons learned.

2. Rationale for Development of the Payload

2.1. Mars Surveyor 2001 Rover and Mars Exploration Rover

[4] The Mars Surveyor 2001 rover was conceived to conduct remote-sensing science and in situ science at specific targets. Additionally, rock cores and soil samples would be acquired and stored on board [Myrick *et al.*, 2000] as a precursor to future sample return missions. Its design was to (1) support the Athena Science Payload, (2) traverse up to 100 m per sol, (3) provide a navigational accuracy of 10% or better, and (4) provide high-speed computational capability and substantial data storage. The Athena Science Payload for that mission consisted of the components listed in Table 1. In addition, that rover was to carry several other camera systems: (1) Navcam atop the mast for navigation, (2) front and rear Hazcams for hazard-avoidance maneuvering, and (3) Belly-cams under the rover body to monitor MiniCorer operations.

[5] The current incarnation of advanced roving on Mars is the Mars Exploration Rover (MER) Project, which plans to launch two rover missions to Mars in 2003 and have them each operating on the surface of Mars in 2004. The MER Mission rovers each carry a modified Athena Science Payload, summarized in Table 1. The basic concept of a rover capable of conducting remote-sensing and in situ science is retained with the new payload composition.

2.2. FIDO Athena Emulation and Payload Requirements

[6] FIDO is an operational prototype rover, equipped with elements resembling those of the Athena Payload

(Table 1). It is used to simulate the complex surface operations expected of an in situ mobile science platform on another planet, focusing on characterization of the scene, identification of rock and soil targets, approaching the targets, and conducting measurements as well as drilling and verification of cores. This last FIDO capability was included to develop Mars Sample Return Mission operations, or, more generally, to develop the operations scenarios needed on rover sample acquisition and return missions.

[7] The instrument payload on FIDO includes a mast that is stowed on the rover deck when the vehicle is moving and deployed to 1.94 m height for acquisition of stereo imaging and spectral reflectance data. The mast head houses Pancam, a three-band false-color infrared (0.65, 0.74, 0.855 μm) imaging system capable of surveying the terrain in stereo with high spatial resolution for scientific purposes. Pancam imaging provides clues to mineral composition [Arvidson *et al.*, 2002; Jolliff *et al.*, 2002]. These three wavelengths were chosen to yield information on the ferric nature of observed minerals. The Navcam stereo imaging system, which provides low spatial resolution, monochromatic, wide field of view images used for traverse planning, is also included in FIDO's mast head. These systems are similar to those that were intended for the Mars Surveyor 2001 mission [Squyres *et al.*, 2000; Bell *et al.*, 2000b] and that are now planned for the Athena Payload on the MER Missions. However, the angular resolution of the FIDO imaging system is not quite as good as planned for the Athena Payload, and the number and wavelength coverage of the FIDO Pancam bands is less than what is planned for the Athena Pancam. The Infrared Point Spectrometer (IPS) on FIDO is bore-sighted with Navcam and acquires spectral radiance information over wavelengths from 1.3 to 2.5 μm with a spectral resolution of $\sim 13 \text{ cm}^{-1}$. The IPS can be

used in both a point mode and a mode in which a suite or raster of data is acquired to form an image cube. The Miniature Thermal Emission Spectrometer (MiniTES) was to be flown on the Mars Surveyor 2001 Rover and will be flown on the MER Missions, with a wavelength coverage from 5 to 29.5 μm and a spatial resolution choice of either 20 or 8 milliradians [Christensen *et al.*, 2000]. The MiniTES, however, was too expensive to replicate for FIDO. The less expensive IPS was built to simulate joint use of imaging and point hyperspectral data.

[8] A 4-degree-of-freedom arm is included on the front of the FIDO Rover. The end effector on the arm is the mounting point for a color microscopic imager and an ^{57}Fe Mössbauer Spectrometer. The Mars Surveyor 2001 rover arm would have carried similar instruments for obtaining rock and soil data, with the addition of a calibrated Alpha Proton X-ray Spectrometer (APXS) and a Raman Spectrometer [Wang *et al.*, 2000]. The APXS will not work in Earth's atmosphere because the higher density of terrestrial atmospheric constituents dominates the observed elemental abundance. A Raman Spectrometer was not available for inclusion on FIDO for the field tests.

[9] The MiniCorer on FIDO is an Athena prototype rock drill directly mounted on the rover body. It is pitched down from its horizontal stow position to acquire a 0.5-cm-diameter by up to 1.7-cm-long core. The equivalent dimensions for the Athena MiniCorer were to be 0.8×2.5 cm [Myrick *et al.*, 2000]. Cameras mounted on the underside, or "belly," of FIDO monitor drill deployment. Similar belly cameras were to be used on the Mars Surveyor 2001 Rover. For FIDO the core can be extracted from the rock and examined with the Microscopic Imager. Once a core's presence is confirmed, it can be either ejected or kept and placed in a caching tube. For the FIDO Rover the Microscopic Imager and Mössbauer Spectrometer can also be placed against rock and soil targets to acquire close-up views and information on iron oxidation state and the mineralogy of iron-bearing phases. For the Mars Surveyor 2001 Rover all three spectrometers and the Microscopic Imager would have been able to be placed against the MiniCorer bit end to make measurements of the rock core tips. The MER Mission rovers will each have a Mössbauer Spectrometer, an Alpha Particle X-ray Spectrometer (still called APXS, but without proton mode), and a Microscopic Imager mounted on a 5-degree-of-freedom arm, along with a drill-like tool for abrading rock surfaces (Table 1).

[10] Hazard avoidance camera pairs, or Hazcams, on FIDO are located on the front and back of the vehicle to acquire stereo images and terrain maps of the areas to be traversed. Onboard autonomous hazard-avoidance software is used to judge whether obstacles are too high to be successfully traversed. If judged to be a hazard, the software commands the vehicle to search for and implement a traverse around the obstacle while still trying to reach a waypoint designated remotely by the science team. Similar systems were planned for the Mars Surveyor 2001 Rover and will be used on the MER Mission rovers.

[11] Thus, with the exception of the APXS, the FIDO rover instrument suite provides a useful emulation of the MER Missions' instrument suite and can be used to simulate MER Mission rover operations scenarios with

good verisimilitude. In addition, MiniCorer integration with FIDO allows simulation of Mars sample return operations scenarios.

2.3. Rover Instruments and Science Instruments

[12] This paper describes the "science instruments" only; we do not discuss the navigation camera stereo pair (Navcam) or the hazard avoidance cameras (front and rear Hazcams and Bellycams). These operational stereo cameras are certainly used for scientific target acquisition; for example, the Navcams are used to take situational panoramas around the rover, and the forward Hazcams also contribute to placement of the robotic arm onto targets of scientific interest. Of course, all images from an unknown terrain can be interpreted for geologic and geomorphic information. The use of these other cameras is discussed by Arvidson *et al.* [2002].

3. Pancam

3.1. Description

[13] Pancam consists of a pair of off-the-shelf black-and-white CCD cameras with a pair of custom-designed liquid crystal tunable filters (LCTF) (Figure 1a). The Pancam cameras are Marshall Electronics V-1208 multifunction miniature black and white cameras with 512×492 arrays. The cameras were selected for their small size, modest power consumption, and, most important, the ability to disable automatic exposure. A goal of these cameras was to produce some degree of absolute radiometry in each of the selected filters. With automatic exposure enabled, this would be impossible.

[14] The field of view of Pancam is ~ 14 degrees square using an off-the-shelf 25-mm lens. Adjustment for nominal outside exposure levels was done by setting the manual iris control to $f/10$. This also set the depth of focus so that objects are in focus from 1.5 to 10 m.

[15] One LCTF was placed at the lens on the object side of each camera/lens assembly and allows operation at 650, 740, and 855 nm. Bandwidths are 18, 25, and 28 nm, respectively (Figure 2). Temperature sensors were also installed on each filter assembly and on each camera board near the detectors. LCTF and detector temperature knowledge allows for further calibration of the system.

[16] Both camera/lens assemblies and LCTFs are mounted on a stiff base plate that serves as an optical bench. This bench minimizes angular displacement as a function of temperature and enables stereo image pair acquisition in spite of mast vibration. The supporting structure holding the lens/camera assembly on the optical bench also locks the iris and focus adjustments on the lens. This prevents any mis-adjustments during field operations. The optical axis of each camera/lens assembly was toed-in by 0.677° toward the opposite camera to maximize the stereo data return. Precision alignment pins in the optical bench allow the cameras and filters to be removed and replaced without affecting optical alignment. The horizontal separation between axes is 15 cm.

3.2. Characterization and Calibration

3.2.1. Spectral Calibration

[17] Band passes for the FIDO Pancam LCTF filters are illustrated in Figure 2. Note the leakage between the 650-

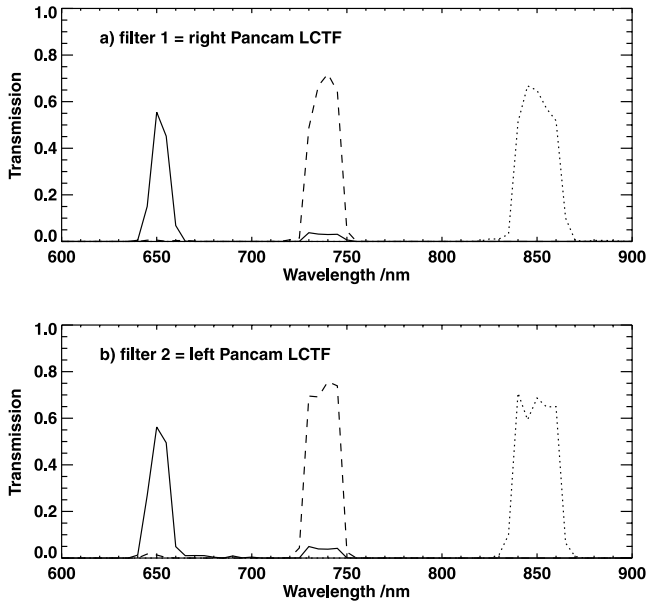


Figure 2. (a) Right, or Pancam filter 1, and (b) left, or Pancam filter 2, measured transmissions.

and 740-nm filter settings. The amount of light leaking through can be estimated analytically from the curves by comparing the area under each main band pass with the area under the outlying “bump.” This gives an estimate of the amount of light in each band that consists of “out of band” photons.

3.2.2. Radiometric Calibration

[18] Each FIDO panoramic camera was aligned with an illuminated Spectralon target, and images of the target were taken while ensuring that each camera’s field of view (FOV) was filled by the target. The target was illuminated by a 1000 W National Institute of Standards and Technology (NIST)-

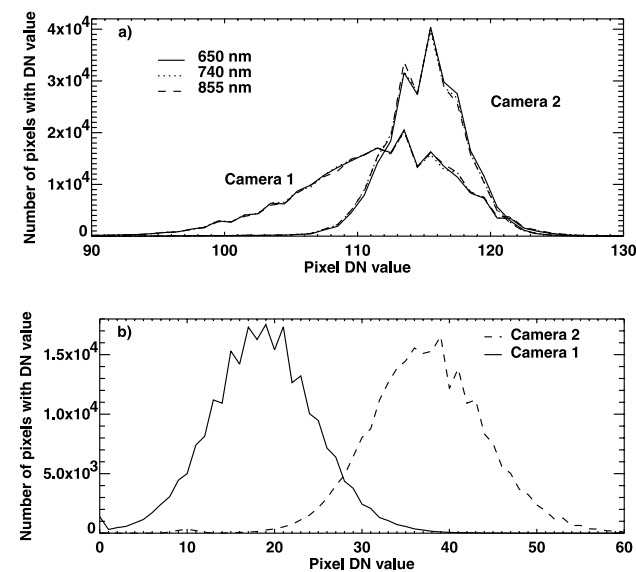


Figure 3. (a) DN distributions of the Pancam cameras in response to viewing illuminated spectralon target panel. (b) Pancam camera dark image DN distributions. Cameras 1 and 2 are the right eye and left eye, respectively.

traceable calibrated irradiance bulb at the standard 50-cm distance. Images of the target were taken with each camera at all three wavelengths in order to determine the optical transfer function (OTF) of the cameras (after taking into account the filters). The image data were processed to yield data number (DN) distribution data, shown in Figure 3a. For each channel and camera, mean illuminated and dark DN values were determined. Dark current data are shown in Figure 3b. The signal from each camera for each channel can be defined by the following equations (which integrate over the filter band pass):

$$\begin{aligned} \text{DN}_{650} - \text{DN}_{\text{dark}} &= \int_{650 \text{ Band pass}} T_{650}(\lambda)L(\lambda)\text{OTF}(\lambda)d\lambda \\ &+ \int_{740 \text{ Band pass}} T_{650}(\lambda)L(\lambda)\text{OTF}(\lambda)d\lambda \quad (1) \end{aligned}$$

$$\begin{aligned} \text{DN}_{740} - \text{DN}_{\text{dark}} &= \int_{650 \text{ Band pass}} T_{740}(\lambda)L(\lambda)\text{OTF}(\lambda)d\lambda \\ &+ \int_{740 \text{ Band pass}} T_{740}(\lambda)L(\lambda)\text{OTF}(\lambda)d\lambda \quad (2) \end{aligned}$$

$$\text{DN}_{855} - \text{DN}_{\text{dark}} = \int_{855 \text{ Band pass}} T_{855}(\lambda)L(\lambda)\text{OTF}(\lambda)d\lambda, \quad (3)$$

where $L(\lambda)$ is the radiance of the target at wavelength λ , $T_i(\lambda)$ is the transmission of filter i at wavelength λ , and $\text{OTF}(\lambda)$ is the camera optical transfer function at wavelength λ .

[19] With a known Spectralon target radiance $L(\lambda)$, the OTFs for each camera and channel can be found. The 855-nm case is simplest: the difference between the illuminated and dark values is divided by the expected radiance coming into the camera, taking into account the spectral radiance of the source and the transmission of the filter. The 650- and 740-nm cases must be solved simultaneously. Finally, the relative responsivity of each camera/channel combination can be calculated, assuming the 855-nm channel as a reference. These results are presented in Table 2. The camera OTF is in units of: $\text{DN cm}^2 \text{ nm sr } \mu\text{W}^{-1}$.

[20] The spectral analysis constrains the amount of leakage between the 650- and 740-nm channels. The radiometric results depend on knowledge of this relationship. To determine the input radiance for each channel on each camera, (3) can be solved alone, while (1) and (2) should be solved simultaneously. Use of a calibration target with a known reflectance may provide a check on the stability of the camera OTF values with time and temperature.

3.2.3. Photometric Calibration

[21] A separate field characterization of Pancam was carried out to determine its photometric performance when integrated onto FIDO’s mast and operating in an outdoor

Table 2. Pancam Camera Parameters

	Mean DN		Dark Current		OTF (Conversion Factor)		OTF Relative to 855-nm Band	
	Cam 1	Cam 2	Cam 1	Cam 2	Cam 1	Cam 2	Cam 1	Cam 2
650	113	115	19	38	14.7940	12.6247	3.3701	3.9448
740	113	115	19	38	5.8489	5.0859	1.3324	1.5891
855	113	115	19	38	4.3897	3.2003	1	1

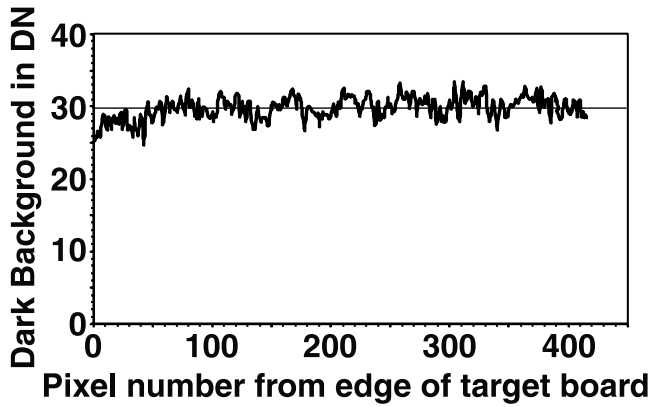


Figure 4. Dark background for right Pancam camera. Each point is the average across a strip 8 pixels high crossing the region in the right Pancam camera where the target board was imaged. The horizontal line is the average of 415 measurements. The banding is clearly visible.

lighting environment. Gray level targets produced on a laser printer were set up in the JPL Mars Yard, and Pancam images were acquired. Reflectivities of the targets with respect to white paper were measured with a Pritchard photometer operating at around 550 nm. We use the term reflectivity in this paper when describing calibrations, whether for the Pancam, the Microscopic Imager, or the Pritchard photometer, to refer to the ratio of the signal obtained from the target patch to the signal from the white paper or other reference target. The reflectivities measured with the photometer are considered valid for calibration at Pancam wavelengths because the carbon-based toner of the laser printer has a reasonably flat reflectance spectrum into the near infrared. The photometric calibration presented here did not take into account the leakage between the 650- and 740-nm channels, but dealt only with each image channel on its own.

[22] Pancam exhibits a dark background that is lower at the side of the frames and shows vertical banding, as shown in Figure 4. The average dark background for the portion of the Pancam frame occupied by the calibration targets was 22.3 DN for the left camera and 24.4 DN for the right camera. Target reflectivities, R_t , were determined by correcting for the dark background and taking the ratio of the target image data number (DN) to the average DN of four adjacent blank targets using a 16×16 pixel sampling window. When the reflectivities measured with Pancam are plotted against those measured with the Pritchard photometer (Figure 5), most of the points fall close to a straight line, but not along the ideal 1-to-1 correspondence. The reflectivities from both Pancam cameras agree closely for all targets at all three wavelengths, suggesting that the Pancam data can provide their own internal reference. The reflectivities derived from 855 nm Pancam data were

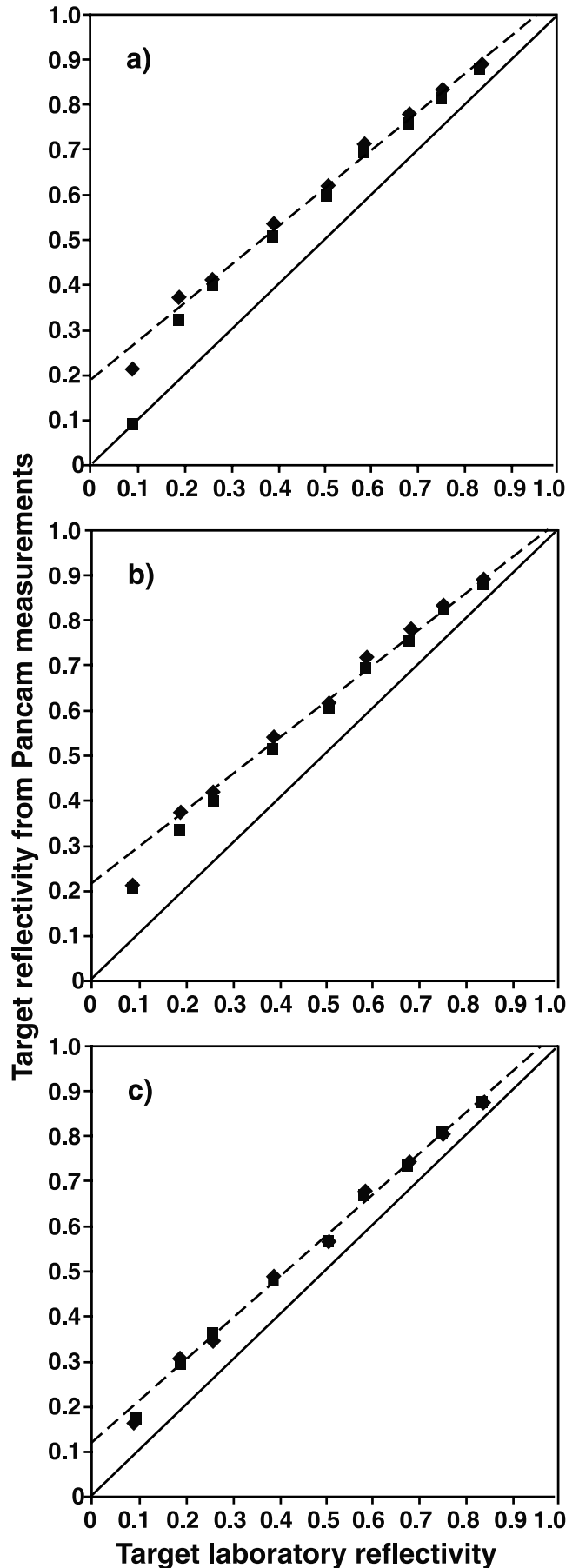


Figure 5. (opposite) Reflectivities calculated from Pancam data with dark background correction versus laboratory reflectivity at (a) 650 nm, (b) 740 nm, and (c) 855 nm. Diamond symbols are for the left Pancam camera, and box symbols are for the right Pancam camera.

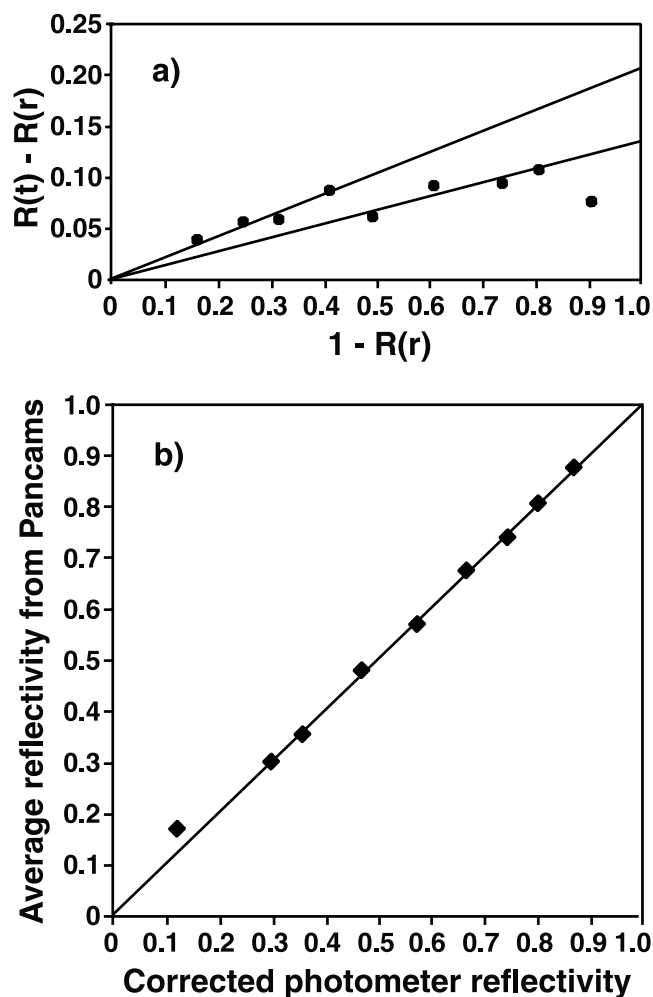


Figure 6. (a) Correction to the photometer reflectivity determined from the average of the left and right Pancam measurements at 855 nm by plotting $R_t - R_r$ versus $1 - R_r$ (see text). (b) Average reflectivity from the 855-nm Pancam data versus corrected photometer reflectivity.

selected as a reference because they agree most closely with those determined by the photometer. The photometer data can be brought into agreement with the Pancam data by applying a correction of the form $R_t = R_r + m[1 - R_r]$, where R_t is the reflectivity of the targets as determined from the Pancam data, R_r is the reference reflectivity determined with the Pritchard photometer, and m is the correction parameter. The quantity m can be determined by plotting $R_t - R_r$ versus $1 - R_r$, as shown in Figure 6a, and finding the slope of a line fit to the data. The data in Figure 6a could be taken as a single group but are more accurately described by breaking them into two groups with separate slopes. When these correction factors are applied to the corresponding 855 nm data points, the result is Figure 6b. The small corrections result in very close agreement between the photometer measurements and the Pancam results at 855 nm.

[23] When the 650- and 740-nm reflectivities are plotted against the average 855-nm reflectivities, they still do not plot on the 1-to-1 diagonal. Either scattered radiation from the general illumination or the 650-nm/740-nm leakage

produces an additional background. A correction can be calculated from $b = (T - R_r)/(1 - r)$, where b is the background, T is the target reading, R_r is the reference reading, and r the 855-nm reflectivity. The corrections determined for the 650- and 740-nm wavelengths are listed in Table 3, and corrected reflectivities from each Pancam camera are shown in Figure 7.

3.2.4. Resolution

[24] To determine the Pancam resolution under field conditions, the modulation transfer function, or MTF, was measured. A laser printer was used to produce a resolution target consisting of seven black lines of equal thickness separated by equally wide gaps. The target was tapered to provide a range of spatial frequencies for the resolution analysis. Pancam frames were acquired with the target board oriented both horizontally and vertically. Sections were taken across the images of the targets at intervals along their length, and the frequency, minimum DN, and maximum DN of each section were determined. The modulation ratio is calculated as $(DN_{\max} - DN_{\min})/(DN_{\max} + DN_{\min})$, where DN_{\max} is the maximum DN and DN_{\min} is the minimum DN of the cross section. Figure 8 shows the MTF obtained by plotting the modulation ratios as a function of spatial frequency for the left Pancam camera using the 740-nm LCTF filter. The resolving power of the Pancam cameras is slightly better in the horizontal direction than the vertical and slightly better for the right camera than the left. The transfer curves for the 740-nm wavelength typically fall to half of their zero frequency value before the spatial frequency has reached 0.2 cycles per pixel.

3.3. Operations

[25] During operations in the JPL Mars Yard and in the field, Pancam has been used for detailed mapping of science targets. Typically, at the beginning of some operational trial, Navcam panoramas are acquired for planning purposes and to delineate interesting areas. Next, higher-resolution Pancam data are acquired in false color for specific targets, although in some cases full panoramas are also acquired because of the rich array of targets. The Pancam image data are acquired at the same time as images of the radiometric calibration target mounted on FIDO's deck. The calibration target is a Mars Pathfinder spare, and it is described by *Smith et al.* [1997]. In past field tests, Pancam imager data have not been quantitatively interpreted, and the dominant mode of analysis of Pancam data has been the generation of false-color IR composites and the use of those products to define morphology and rock types. An example false-color mosaic is shown in Figure 9. The Pancam 855-, 740-, and 650-nm filter images are assigned to red, green, and blue, respectively. Prior to combination the raw digital images are normalized, and the 855-nm filter images are contrast enhanced to achieve a more "realistic" false-color color balance.

Table 3. Pancam Reflectivity Corrections Relative to 855 nm

Filter, nm	Camera Correction Value, DN	
	Left	Right
650	-21.7	-11.1
740	-44.2	-37.0

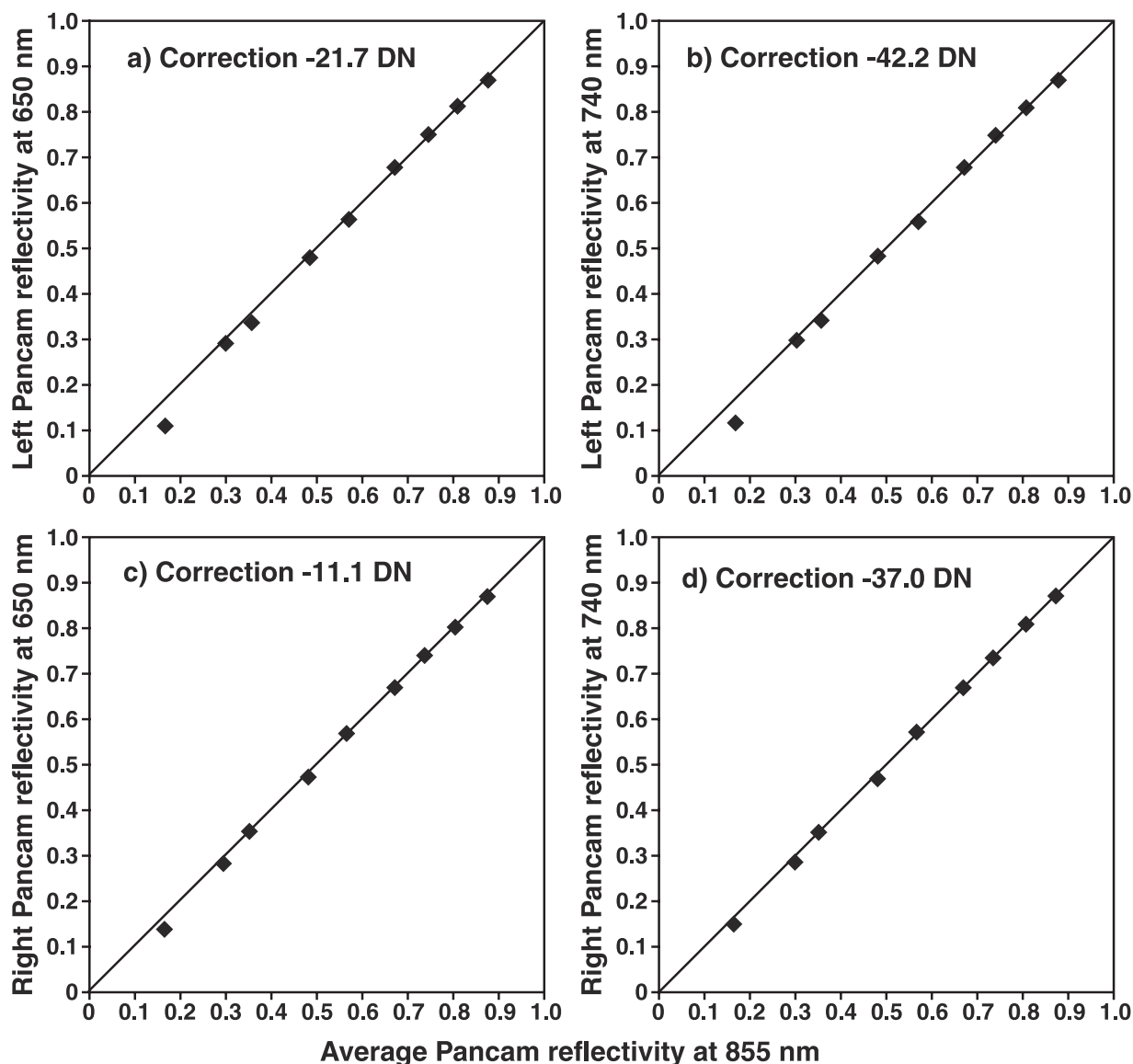


Figure 7. Corrected reflectivity versus average reflectivity at 855 nm: (a) left Pancam camera at 650 nm, (b) left Pancam camera at 740 nm, (c) right Pancam camera at 650 nm, and (d) right Pancam camera at 740 nm.

[26] The FIDO Pancam provides an effective, low-cost emulation of the MER Pancam. The wavelengths selected for FIDO Pancam were selected to enable iron mineralogy classification for operational selection of interesting targets for in situ science. The radiometric and photometric calibrations performed should allow some spectral interpretation of iron oxidation state ($\text{Fe}^{2+}/\text{Fe}^{3+}$) in a fashion analogous to that used for rock and soil mineral identification on Mars Pathfinder by *Bell et al.* [2000a] and *Morris et al.* [2000].

4. IPS

4.1. Description

[27] Since the instrument mast payload was limited to ~ 1 kg, the Infrared Point Spectrometer (IPS) design placed only the foreoptics on the mast with the rest of the IPS inside the rover body, piping the light down the 1.94-m mast with an optical fiber. The Brimrose Corporation customized one of

its spectrometers to use sunlight instead of an internal light source. By putting the commercial detector's acousto-optical tunable filter (AOTF) into the detection path, Brimrose was able to redesign their mechanical and electrical package to meet the FIDO accommodation envelope and acquire near-infrared reflectance spectra in sunlight. Figure 1b schematically illustrates the IPS optics and electronics. The IPS electrical package includes a DOS-based PC electronics stack comprising a PC board, a radio-frequency (RF) board and amplifier, an analog-to-digital (A/D) board, and two interface boards. Separate from the PC stack are the thermoelectric cooler controller board and the power supply board.

[28] The acousto-optical filter is an electro-optical device that can electronically tune its transmission wavelength by changing a RF signal applied to the AOTF crystal. The applied acoustic wave sets up a periodic grating in the crystal by modulating the crystal lattice spacing [*Harris and Wallace, 1969; Tran, 1992*]. Incoming light is diffracted by

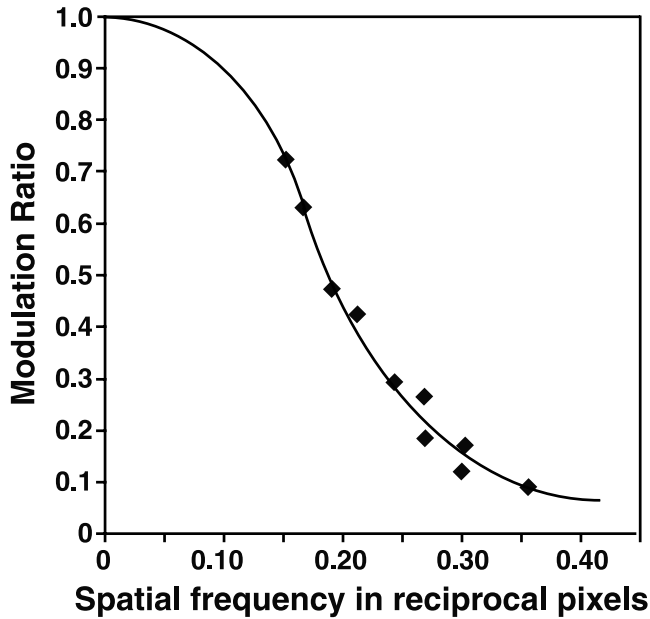


Figure 8. Typical example of Pancam modulation transfer function: horizontal modulation ratio versus spatial frequency for the left Pancam at 740 nm.

the induced grating with a narrow spectral band pass. The applied RF signal is varied to progressively alter the grating spacing in order to sweep the entire IPS band pass (1.3–2.5 μm) across the infrared detector slit. The IPS uses an extended Indium-Gallium-Arsenide, thermoelectrically cooled, infrared detector.

4.1.1.1. IPS Commanding

[29] The IPS electronics are controlled and commanded from the software running on the PC within the IPS. The input parameters for the command to acquire a spectrum, and their ranges are listed in Table 4. The “gains” 1, 2, 4, and 8 are not in fact multiplicative factors, but merely labels, corresponding to nominal multiplicative factors of 1, 5, 10, and 43.1, respectively. However, since the gain amplifies the noise by the same factor, the gain setting is left at 1 for all IPS field applications. To have the minimum noise after the electronics upgrades described later were made, various instrument electrical settings were adjusted so that bright sunlight would reach a maximum of $\sim 20,000$ DN in IPS spectra. The co-adds setting is the controlling factor in reducing the noise at the expense of integration time. IPS noise behavior is discussed in section 4.4. The proper way to reduce the signal noise is to integrate the light reflected from the target for a longer time. Because the IPS acquires a spectrum by sweeping across individual wavelength bins, longer integration times are effectively commanded by the number of spectra acquired, or “co-adds”, N . The IPS sums N individual spectra and then divides by N .

4.1.1.2. IPS Pointing

[30] The IPS was boresighted with Pancam and Navcam after the entire mast head was assembled. The IPS spot is located within the Pancam field of view by projecting an external laser through the IPS fiber and foreoptics onto the IPS Spectralon calibration target mounted on FIDO’s hard-back. An opaque mask with a round hole that is approximately the size of the IPS spot at the target range is aligned



Figure 9. False-color representation of Pancam images in which blue, green, and red are assigned to 650-, 740-, and 855-nm channels, respectively. Individual channels were normalized prior to combination. The image is a mosaic of nine Pancam frames taken along a channel wall at the Silver Lake test site.

with the laser beam. Once the IPS spot is centered in the hole, the mast actuator positions are noted, and Pancam and Navcam images are taken to document which pixels are occupied by the IPS spot. This targeting needs to be repeated with the same frequency as the cameras are recalibrated. Targeting the IPS with the Web Interface for Teleoperated Science (WITS) is done relative to Navcam range maps [Backes *et al.*, 1997, 2000; Backes and Norris, 2001]. This is required because light flux limitations of the laboratory test setup relative to the narrow-band LCTF infrared filters limit Pancam range-calibration indoors. IPS spot locations are therefore not correctly assigned on Pancam images in WITS, and Navcam images of the IPS target should be used instead.

4.2. Additional Developments

4.2.1. Thermal Design

[31] In order to meet the thermal requirements (temperature $< 60^\circ\text{C}$) for the FIDO field trials [Arvidson *et al.*, 2000, 2002], we made extensive modifications to the electronics.

Table 4. IPS Input Parameters

Parameter	Possible Values	Standard Setting
Minimum wavelength, nm	1300–2499	1300
Maximum wavelength, nm	1301–2500	2500
Wavelength step size, nm	1–1200	1
Number of spectra, co-adds	integer ≥ 1	100, 1000
“Gain”	1, 2, 3, 4	1

Table 5. IPS Optical Fibers

Fiber Name	Manufacturer	Specifications	Usage
Flexible Fiber	Fiberguide	low OH silica; 400- μm core; plastic cladding; NA ^a = 0.4; 2.5- and 3.0-m lengths	April 1999
Cyborg Fiber	Amorphous Materials	As ₂ S ₃ ; 600- μm core; NA = 0.5; 2.5- and 3.0-m lengths	April 1999
Purple Fiber	Galileo Corp.	Low OH silica 500 μm core NA = 0.2 3.5 m lengths	October 1999
Fiber Bundle	Thor Labs	Fluoride glass; bundle of seven 160- μm core fibers; 4.3-mm PVC monocoil over PEEK tubing; NA = 0.28; 3.0-m lengths	May 2000

^aNA, numerical aperture.

The FIDO electronics box reached temperatures as high as 60°C, and we discovered several problems with the IPS at elevated temperatures. Most significantly, the signal from this modified laboratory instrument varied considerably with temperature in our field applications, whether for a dark level measurement or an illuminated one. To correct this, we made two critical modifications that eliminated most thermal drift. First, the reference voltage for the A/D converter was very temperature sensitive. As a result, the conversion gain varied with temperature. This was stabilized with a new circuit design, which we used to bypass the original reference voltage. Second, the AOTF is actually modulated at ~19 kHz, and the signal is detected synchronously through passive fixed filters. The modulation frequency was also temperature sensitive, so that as it shifted, the signal was actually being detected in the wings of the filters, reducing the signal. A phase-locked crystal oscillator solved this problem.

4.2.2. Optics Design

[32] After the first field trial in April 1999 [Arvidson et al., 2000], analysis of the IPS data showed that we needed more signal-to-noise ratio (SNR), particularly in the 2.3–2.5 micron region, which contains key spectral features related to combination and overtone vibrations associated with clays and carbonates, two mineral types of intense interest for Mars, and, by association, at the terrestrial Mars-analog field test sites. The limiting *F* number of the system was that of the spectrometer; there was no value to using larger *F* number collection optics as we could not effectively couple the extra photons into the spectrometer. However, the data convinced us that more SNR was required, so Brimrose modified the spectrometer to decrease the *F* number to *f*/1.3 from *f*/3. The *f*/3 system is shown in Figures 1a and 1b. The decreased *F* number now required new foreoptics and new fibers to transmit the signal to the spectrometer in the FIDO rover. Since small *F* number refractive optics get large quickly and are more sensitive to alignment errors, we designed an all-reflective *f*/1.3 system. The system was fabricated with diamond-turned aluminum that had all the alignment and assembly features machined into each optical element.

4.3. Optical Fibers

[33] The selection of optical fiber to carry the infrared photons from the foreoptics to the Brimrose detector inside FIDO required significant trial and error. The requirement of maximum infrared transmission, in particular in the region beyond 2.2 microns, where significant mineral vibrational

features appear, is somewhat at odds with the requirement for mechanical robustness to support the repeated deployments of FIDO’s mast. Fibers used during FIDO field tests are listed in Table 5. The low-OH silica fiber from Galileo Corporation (“Purple Fiber”) used in development turned out to have better infrared transmission beyond 2.2 microns than the low-OH silica fibers from Fiberguide (“Flexible Fiber”). The As₂S₃ “Cyborg Fiber” (named because of its coiled metallic cladding), which had good infrared transmission, proved too brittle for the rigors of our field trials. Ultimately, a bundle of seven small fluoride glass fibers was selected. This design combined the appropriate material for infrared transmission with a packaging that had proven itself robust enough to survive rover field use. A comparison of spectra from the various fibers is shown in Figure 10. The Fiber

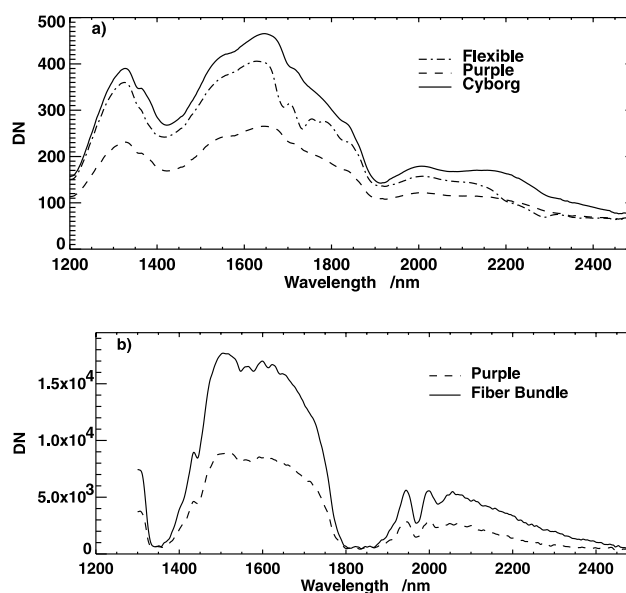


Figure 10. IPS fiber comparison of laboratory test spectra: (a) Purple, Cyborg, and Flexible Fiber performance with the IPS compared in the laboratory using a spotlight illuminating a Spectralon target (13 April 1999), (b) Purple Fiber and Fiber Bundle Spectralon spectra taken in sunlight on FIDO in the JPL Mars Yard (21 March 2000). Note by comparing Figure 10b to 10a that the Fiber Bundle performance is equivalent to the Cyborg fiber. The Fiber Bundle was much more mechanically robust in field usage.

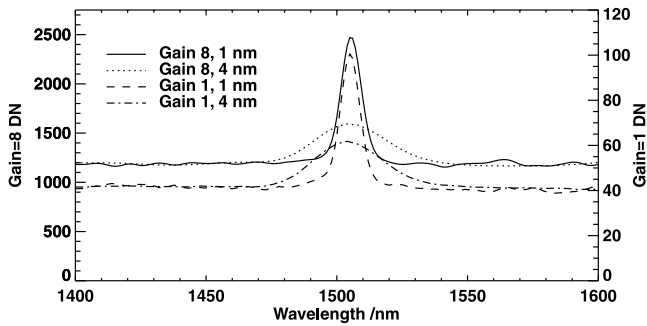


Figure 11. Response of IPS to 1-nm-wide 1500-nm monochromator input. Ordinates are data number (DN) readings for IPS “gain” input setting of 8 on the left-hand side and of 1 on the right-hand side.

Bundle transmission is comparable to that of the Cyborg fiber, while being thoroughly robust for FIDO applications.

4.4. Characterization and Calibration

4.4.1. Spectral Calibration

[34] A monochromator was used to produce a 1-nm-bandwidth light source for spectral calibration of the FIDO IPS. The wavelength calibration of the monochromator itself was checked using a Hg vapor lamp which produced lines of known wavelength. The IPS response was measured with 1- and 4-nm sample spacing, with gains of 1 and 8. A typical instrument response (for a 1500-nm input) is shown in Figure 11. There is a measurable offset between the wavelength of the input and the IPS reported results, and further, the full-width half maximum of the response varies strongly with wavelength sample spacing. The amount of offset, however, is independent of both sampling and gain settings. The repeatability of these results was quantified by determining the standard deviation of all measurements. These results are summarized for the entire spectral range in Figures 12 and 13. Reduced monochromator lamp output and decreased grating efficiency are primarily responsible for the poorer repeatability at longer wavelengths. Reduced IPS sensitivity at these longer wavelengths also reduces SNR, affecting the repeatability of the measurements. The values of the offsets changed after the modifications to the electronics to reduce noise were applied (Figure 12b). The offsets are entirely correctable in postprocessing for all IPS data sets.

4.4.2. Radiometric Calibration

[35] The purpose of the radiometric calibration was to determine the optical transfer function (OTF) of the IPS instrument. A NIST-traceable calibrated light source was used to illuminate a spectralon panel of known reflectance. This combination produced a target of known radiance which was observed with the IPS through the $f/3$ foreoptics and fiber. The response of the instrument to the essentially blackbody illumination is shown in Figure 14a. The dark current levels are independent of the sampling spacing but change with gain settings. The dark current for the data sampled at 4-nm spacing is shown in Figure 14b.

4.4.3. IPS Noise and Thermal Stability

[36] Two characteristics of signal noise are important on the IPS: the level of the noise floor or “dark current,” and the variation, or repeatability, of any spectral (or dark

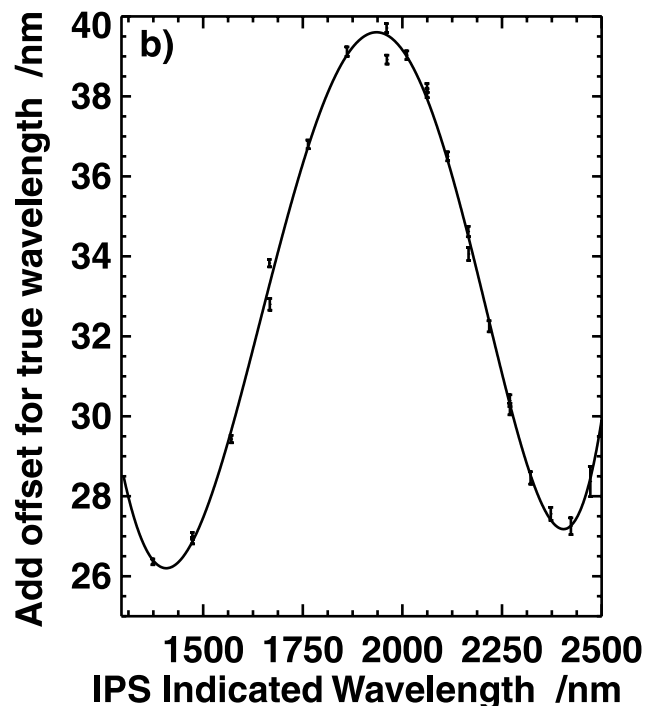
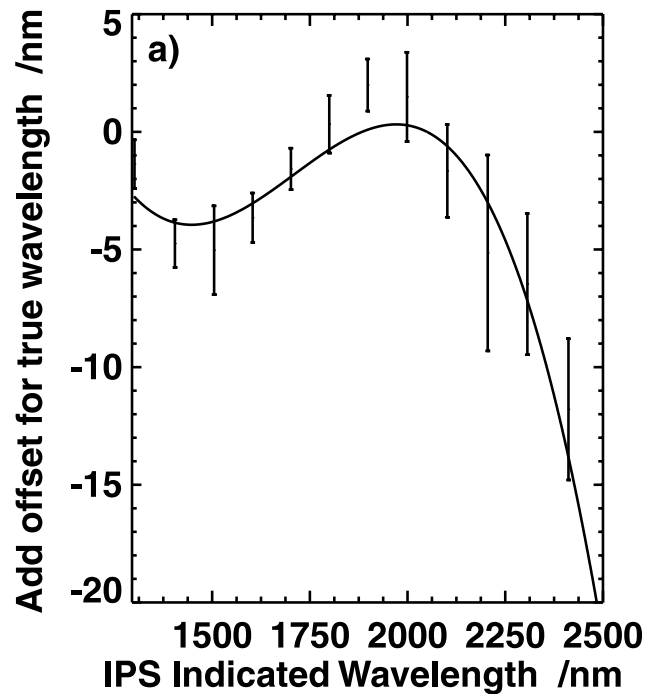


Figure 12. IPS spectral offset for 1-nm, gain = 1 case; results are independent of gain and sampling. (a) Offsets prior to noise modifications made mid-1999, where the error bars are the standard deviations from five measurements of the offset at each wavelength, and (b) offsets for October 1999 onward, where the error bars on the fits are 3 times the fit RMS uncertainty of the monochromator center wavelength. Lines in Figures 12a and 12b are best fit cubic and quintic polynomials, respectively.

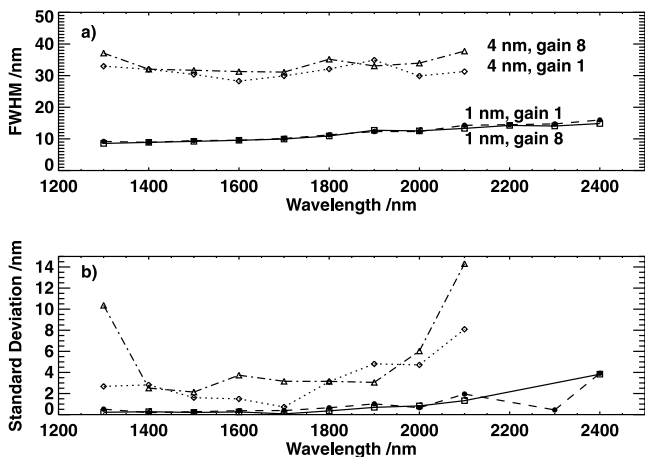


Figure 13. (a) Full-width half maximum (FWHM) response of IPS to 1-nm input. Results vary with gain setting and sampling step size (wavelength sampling every 1 or 4 nm). (b) Repeatability of IPS FWHM measurements, quantified as standard deviation of test measurements. Measurements at ends of range are subject to greater uncertainty in bandwidth. Line styles in Figure 13b are the same as in Figure 13a.

current) measurement. The level of the noise floor is determined by settings in the electrical circuits on the interface board and is adjusted to an appropriate level. Prior to optimizing the thermal design, which took place in mid-1999, the noise floor would change, and generally get lower, as the electronics temperature increased. The IPS optics and electronics were tested for thermal stability in a Bemco thermal chamber following the thermal stability modifications described in section 4.2 were made, following the initial field testing (April 1999). The actual gain stability

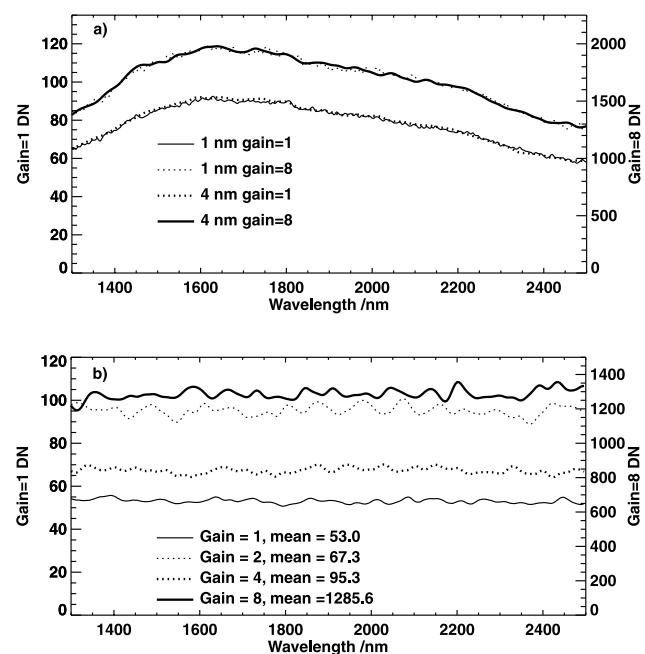


Figure 14. (a) IPS response to calibrated radiance source. (b) IPS dark current for data sampled every 4 nm for various gains. The dark current is independent of sampling.

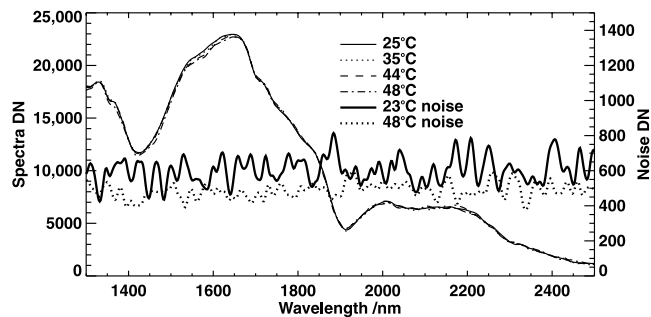


Figure 15. IPS thermal tests of electronics and optics in Bemco thermal chamber after the electronics upgrade made in late 1999. The left-hand ordinate shows data numbers (DN) for the illuminated spectra, and the right-hand ordinate shows DN for the dark spectra. The signal from the optics to the detector was transferred with the Flexible Fiber. The DN levels for the illuminated spectra are higher than those in Figure 12a because of the electronics modifications. Note that the water bands at 1400 and 1900 nm do not saturate over the short distance from the optics to the target in the laboratory setting.

with temperature that was achieved after the modifications is shown in Figure 15. The signal noise shown in Figure 15 is typical for spectra taken with the number of co-adds, $N = 100$. We have observed that the signal noise is random: the ratio of the root-mean-square variation of the dark current relative to its mean for two different values of N , N_1 , and N_2 goes as the square root of the ratio of the N_1 to N_2 .

4.5. Operations

[37] IPS operations on FIDO are commanded via WITS and are fully coordinated with Pancam operations and operations of the rest of the integrated instrument payload. They are also coordinated via WITS with rover position and mobility requirements [Backes and Norris, 2001]. During the field tests the IPS data were always acquired with 1-nm-wavelength sample spacing and with gain $G = 1$. Co-add settings were typically $N = 1000$ but ranged from $N = 500$ to $N = 5000$.

4.5.1. IPS Power Management

[38] For all operations in 1999 and 2000 the IPS had to be turned on separately by flipping switches inside FIDO's payload electronics bay (PEB). Turning on the system at room, or desert, temperature, the IPS would require up to an hour before stable, repeatable measurements could be made because the detector would need to cool and thermally stabilize. With the manual switches the approach was then to have a standby mode where the cooler was always left on, while the rest of the IPS electronics was turned off when not in use. The IPS computer and electronics boot up in a few seconds, and so this manual power management approach was used to reduce the impact of the power-hungry IPS on FIDO's battery supply. Nevertheless, after activating the computer and electronics, the IPS appears to still require a few minutes to properly stabilize its noise floor. Future FIDO operations will allow the IPS to be turned on and off through software commands with WITS.

4.5.2. Data Acquisition

[39] Mineral identification with the IPS requires normalizing rock data to data for a Spectralon target mounted on



Figure 16. A Microscopic Imager (MI) view of garnet sand in FIDO's indoor testing sandbox.

the rover. After subtracting dark current values from the two data sets, the ratio is basically the spectral radiance coefficient. Dark current or noise level acquisition requires detaching the fiber connection at entry to the detector (entry to FIDO PEB) and capping the entry connector with aluminum foil, which is time-consuming during field operations and requires significant handling of the relatively delicate optical fibers. Fortunately, the noise behavior is fairly flat across the IPS bandwidth, and we can use the base levels of the water absorption features in the field spectra (around 1.5 and 1.85 μm) as good samples of the noise spectrum. The IPS data analysis is described by *Arvidson et al.* [2002] and *Jolliff et al.* [2002]. The instrument was used to target acquisition of small arrays of data, which, when analyzed together with imaging observations, provided excellent constraints on mineralogy and rock types encountered during the various operational trials.

5. Microscopic Imager

5.1. Description

[40] The Microscopic Imager (MI) (Figure 1d) provides geologists with close-up views of rock and core samples. An example image of red garnet sand used in FIDO's indoor sandbox is shown in Figure 16. The original goals for the imager were RGB color, 10-mm field of view, and >2-mm depth of field. The field of view requirement was later changed to 15 mm to accommodate the actual selection of an off-the-shelf digital camera and optics. A Philips 2 board color camera providing adequate resolution and light sensitivity with the additional benefit of being able to adjust many operating parameters via the RS232 serial interface is the core of the MI. This camera has a 512×492 CCD array. Using an off-the-shelf 16-mm lens with an 8-mm spacer, the camera can be focused onto an image plane 50 mm from the lens. The resulting field of view is slightly larger than 15 mm by 15 mm. By setting the iris to $f/10$, the depth of focus is 3 mm.

[41] Since it was likely that the subject to be imaged would be shadowed, a source of illumination was added. A ring was designed to supply fairly diffuse light to the imaging area from three incandescent lamps. The ring surface under the lamps was coated with a white diffusing paint. These light-emitting diode (LED) lamps could be switched on and off by the rover. Later, it was decided to add touch sensors to determine when the object was in the imaging plane. Two fingers added to the illuminator ring activate microswitches when the fingers contact a target rock. If only one finger touches, it means the target is not perpendicular to the optical axis. The rover then rotates the imager until the second finger touches the target, placing the target in the MI imaging plane. The finger mechanism consumed enough space on the illuminator ring so that one light had to be removed, leaving a total of two, which proved ample for our application.

[42] The camera power consumption is about 2.5 W. To keep sand and dust contamination out of the camera and off the focal plane, the camera was packaged in a tight-fitting aluminum box. The outside of the box was polished to reduce the absorption of thermal energy and to keep the camera temperature as low as possible while operating. A temperature sensor was also mounted near the detector for monitoring purposes, using FIDO rover telemetry.

5.2. Characterization and Calibration

[43] MI characterizations were performed by analyzing frames taken of a set of custom targets, both opaque and self-luminous. The opaque targets were constructed by mounting sheets printed by a laser printer on poster board. The self-luminous targets were precision gratings placed over a highly diffuse incandescent source. The opaque targets were used for both the photometric and resolution tests. The self-luminous targets were used only for resolution.

5.2.1. Photometry

[44] Issues with the photometric calibration of the MI are whether the built-in illumination of the MI is sufficiently uniform for accurate photometry and whether laboratory measurements of the reflectivity of larger targets with the Pritchard photometer are accurate when applied to the smaller targets used with the imager. As with the Pancam characterization, paper targets consisting of nine gray level patches were prepared. The patches were separated by white areas, which served as reference levels. The uniformity of the target illumination was tested by comparing all the white area signals. A comparison of the MI reflectivities with the photometer reflectivities showed that although the MI reflectivities generally followed the photometer reflectivities, they were significantly higher. A comparison of the individual color reflectivities to the average reflectivity from all three colors (red, green, blue) showed that the photometric ratios for gray targets are very similar in all three colors. Figure 17 plots the digital signals versus the average reflectivities and shows that the digital signals themselves are quite consistent between colors.

5.3. Operations

[45] The MI provides the finest level of detail of all of FIDO's instruments, extending the rover's imaging capabilities down to tens of micrometers. MI images are acquired for targets that have already been examined with other instruments and would benefit from inspection at finer

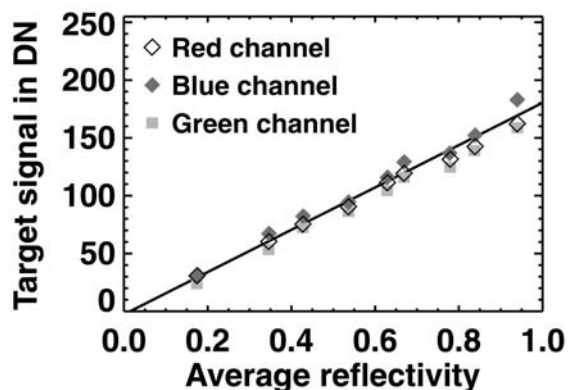


Figure 17. MI digital signals versus the average reflectivities in each color channel from images of the calibration target.

scales. The images are particularly useful for providing textural information to supplement the IPS and Mössbauer data. To acquire a MI frame, the rover is driven into position, the arm is deployed, and the image is acquired. The location of the MI is then documented with front Hazcam images, and the arm is retracted. The MI was used successfully during the April 1999 field test to examine rocks as well as to check for MiniCorer core acquisition [Arvidson *et al.*, 2000]. Examples of MI data from the May 2000 field test are given by Jolliff *et al.* [2002].

6. Mössbauer Spectrometer

6.1. Description

[46] The $\text{Fe}^{2+}/\text{Fe}^{3+}$ ratio provides information on the oxidation state of soils and rocks. The Mössbauer Spectrometer determines the oxidation state of iron and identifies iron-bearing minerals in rocks and soils. Comparison of these oxidation species indicates the extent to which the oxidation state was enhanced during weathering and hence can give insights into the processes involved, the nature of surface-atmosphere interactions, and likelihood of the preservation of organics against the oxidation process. Individual iron oxide and oxyhydroxide minerals have different chemical pathways of formation. For instance, iron oxides or hydroxides formed via precipitation in abundant liquid water will be different from the oxidation products formed via solid-gas reactions. Mössbauer spectroscopy identifies Fe-bearing silicate minerals like pyroxene and olivine as well as ilmenite and other Fe oxides and can also search for Fe sulfates, Fe nitrates, and Fe carbonates.

[47] The MIMOS II Mössbauer Spectrometer used on FIDO (Figure 1e) is a prototype for the Mössbauer spectrometer that will be part of the Athena Payload on the MER Missions [Klingelhöfer *et al.*, 1996; Morris and Klingelhöfer, 1997]. MIMOS II uses a vibrationally modulated source of ^{57}Co in rhenium to illuminate target materials. Backscattered gamma signals are binned according to the source velocity, revealing hyperfine splitting of ^{57}Fe nuclear levels that provides mineralogical information about the target. The instrument uses a mature design developed for operation under Martian surface conditions. Most of its components were originally designed for and tested under

Martian environmental conditions for the Russian Mars 96/98 mission. Functional tests of prototype instruments were in the Mojave Desert on the Rocky 7 rover [Arvidson *et al.*, 1998]. The main parts of the instrument are the Mössbauer drive that moves the ^{57}Co source with a well-known velocity, the γ - and X-ray detectors that detect the backscattered radiation, the microcontroller unit, the $^{57}\text{Co}/\text{Rh}$ Mössbauer source, and the radiation collimator and shielding.

[48] The spectrometer is split into the sensor head, which mounts on FIDO's robotic arm, and the electronics inside the PEB. The sensor head carries the Mössbauer drive with the analog part of the drive control unit, the $^{57}\text{Co}/\text{Rh}$ Mössbauer source, the radiation collimator and shielding, the four PIN-diode detector channels, including pulse amplifiers, and one reference detector channel to monitor the velocity of the drive using a weak ^{57}Co source and a well-known Mössbauer reference absorber in transmission geometry.

[49] The analog signals of the five detector channels are analyzed by discriminators for 14.4-keV and 6.4-keV peaks. Upper and lower threshold values of the discriminators are generated by digital to analog converters (DACs). These values can be changed automatically to follow the temperature drift of the amplifiers. Digital signals from the discriminators are sent to the velocity-synchronized counters whenever a detected pulse is within the specified range. Mössbauer spectra for the two different energies of 6.4 keV and 14.41 keV are sampled separately. Each Mössbauer spectrum consists of 512×3 -byte integers. The pulses from the four counters are added by hardware. Normally, there is one spectrum for each detector. The spectra are sampled into an SRAM of 128 kb size.

[50] Measurements are made by placing the instrument directly against a rock or soil sample. Physical contact is required to provide an optimal measurement distance and to minimize possible microphonics noise on the velocity-modulated energy of the emitted γ rays. The mechanical construction of the robotic arm and the interface limit vibration-induced velocity noise at the sensor head to <0.1 mm/s. A contact plate is mounted at the front part of the sensor head, assuring an optimal distance from the sensor head to the sample of ~ 8 mm. A heavy metal collimator in front of the source provides an irradiated spot of nominally 15 mm (up to 20 mm, depending on actual sample distance and shape) in diameter on the surface of the sample. The average depth of sampling by Mössbauer data is about 100–200 μm .

[51] One Mössbauer measurement takes ~ 12 hours, depending on the phases present in the sample and the total iron content. The temperature variation for one spectral accumulation interval should be less than about $\pm 10^\circ\text{C}$. If larger variations occur, spectra for different temperature ranges are stored separately, resulting in an increase in the total data volume (depending on the number of temperature intervals required) and a decrease of statistical quality for the individual subspectra.

6.2. Characterization and Calibration

[52] In parallel with the measurements of samples, calibration spectra were taken using the reference channel implemented in the instrument. The performance of the Mössbauer Spectrometer can be defined by measurements made in transmission geometry with a Mössbauer source in front of the instrument at a distance of 5 cm and in a

Table 6. FIDO MiniCorer Specifications

Parameter	Value	Comments
Drilling rate	material-dependent	see Figure 2
Dimensions (drill head)	300 × 100 × 65 mm	The pitch-yaw stage is roughly 300 × 100 × 100 mm.
Drill bit stroke	~150 mm	
Power consumption	~30 W	Stall current of the motors is 3 A.
Axial drilling force (weight-on-bit)	150 N	Soft rocks can be drilled at 50 N.
Torque to the bit	~0.15 N m	
Transverse load (drill walk)	Forces in excess of 150 N have been encountered.	These loads can be reduced, somewhat, by an appropriate axial force control.
Control loop	control bandwidth 5 Hz	sampling rate ~100 Hz

backscattering geometry with the source internal to the instrument in its operational configuration. Instrument performance requirements for such purposes are specified for a Mössbauer source strength of 100 mCi for the backscattering mode, 10–20 mCi for transmission mode, an integration time of 10 min for the energy spectra (backscattering and transmission), and an integration time of 10 hours for the Mössbauer backscattering spectrum.

6.3. Operations

[53] The MIMOS II Mössbauer spectrometer was operated fully integrated with FIDO during the April 1999 field test at Silver Lake, California [Arvidson *et al.*, 2000]. Radiation safety procedures required minimizing the number of personnel in proximity to the rover while the Mössbauer was mounted on the FIDO arm. To accommodate this, Mössbauer runs were performed at night with FIDO locked inside the command trailer and a skeleton crew operations team conducting the experiments remotely from the team's recreational vehicle parked nearby. A Mössbauer run consisted of selecting a rock in the field for testing, placing it in the trailer with FIDO, mounting the spectrometer, deploying the robotic arm with the controller box, locking the trailer, and initiating the run remotely (Figure 1e).

7. MiniCorer

7.1. Description

[54] The MiniCorer was developed by Honeybee Robotics, Inc. under the National Aeronautics and Space Administration (NASA) Small Business Innovation Research (SBIR) program [Myrick *et al.*, 2000]. The interface between the MiniCorer and the rover that included mechanical pitch and yaw stage, electrical interface, as well as controls algorithms and their implementations was developed at JPL. During field trials, FIDO's onboard CPU controlled the MiniCorer.

[55] The main requirements imposed on the MiniCorer were (1) the ability to core hard rocks (e.g., basalt) in sets of up to three 25-mm segments in a single bored hole with the total length of 75 mm and a core diameter of 8 mm, (2) the ability to deliver the cores to the science station for inspection, and (3) the ability to eject cores into appropriate receptacles.

[56] Most of the MiniCorer requirements were derived from those of the Mars Sample Return mission. The Martian rover was expected to be lightweight (<300 N on Mars). It had low-frequency structural modes with little damping, and its suspension had deadband and backlash. Table 6 lists the major parameters of the MiniCorer installed on FIDO.

[57] The expected axial drilling force is comparable to the effective weight of a rover on Mars. Thus the coring system must be actively controlled to limit the effect of reaction forces and torques imposed by uncertain interactions between the coring bit and the sampling surface. On Earth, FIDO is significantly heavier than the Martian rover. There was, however, at least one occasion when even FIDO was lifted and moved by the axial actuator of the MiniCorer. The control system was optimized for FIDO, but it can be upgraded for drilling from a lighter platform.

7.2. Characterization and Calibration

[58] To satisfy performance requirements for in situ scientific studies, applied drill forces must track commanded force profiles to within certain specified accuracy. The telemetry data such as penetration rates may be used to derive information about material properties of the sampled rock or substrate drilled. This together with other uncertainties and structural dynamics imposes challenging constraints on the end-to-end operation of the coring or drilling control system. The data in Figure 18 are obtained with the control circuit on from a rover emulator platform. Drilling of sloped rocks and drilling from a very unstable rover have been demonstrated using the emulator in Figure 1c.

7.3. Operations

[59] In preparation for drilling a core with the MiniCorer, the rover is driven into position, and Navcam, Hazcam, and Bellycam images are acquired. The images are downloaded

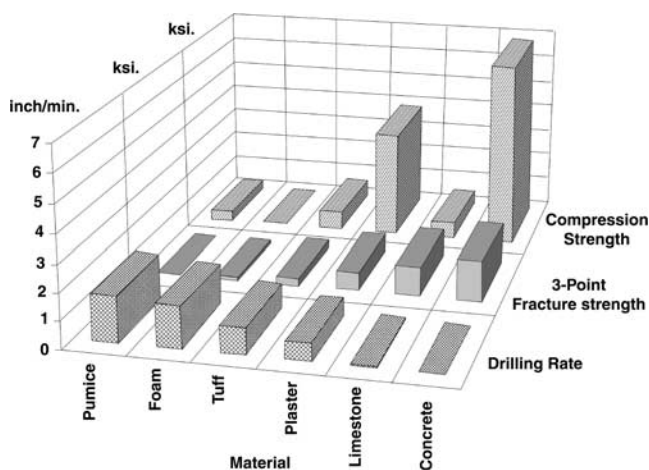


Figure 18. Drilling rates at 30 W for different materials compared with their fracture strength and compression strength.

Table 7. FIDO Instrument Suite Field Usage

Instrument	April 1999, Silver Lake, California	October 1999, Silver Lake, California	May 2000, Black Rock, Nevada
Pancam			
Total images ^a	2700	234	1884
Panoramas	2 × 360°: 684 images 1442 images		1 × 180°: 1458 images
IPS			
Target spectra	37	88	70
Calibration spectra	18	30	37
Microscopic Imager			
Images taken	24	0	28
Mössbauer Spectrometer	6 samples	N/A	N/A
MiniCorer			
Attempts ^b /Success ^c	5/3	3/2	6/1

^a A Pancam image command acquires one image in each eye and each filter, so the numbers listed in the table should be divided by 6 for total number of imaged targets.

^b A MiniCorer attempt is defined here as the initiation of the MiniCorer drill sequence.

^c A MiniCorer success is defined as contact with the designated target and drilling into that target, but not acquisition of a core. See *Arvidson et al.* [2000, 2002] for details of the drilling.

and analyzed to determine whether the rover is in a proper position for sampling. If the MiniCorer can be deployed over the target in a vertical position along the centerline of the vehicle, then FIDO is commanded to proceed with sample acquisition. If these conditions are not met, then a fallback sequence is executed. The fallback sequence is a prestored sequence, typically consisting of Pancam and MiniTES commands, intended to assure that the rover's time is spent productively for the remainder of the sol. A corrective sequence is then determined for execution on the next sol.

8. Instrument Suite Integration

8.1. Instrument Hardware and Software Integration With FIDO

[60] The science instrument hardware integration onto FIDO was intimately associated with the rover's overall configuration and assembly [*Schenker et al.*, 1999, 2001; *Arvidson et al.*, 2000, 2002]. The optical instruments on the mast head required the special design optical bench assembly for stiffness and support and a cover housing for environmental protection of the apparatus under field conditions. The frame-grabber electronics and FIDO PEB electronics were identical for all the cameras, including the science cameras. Accommodation of the IPS, Mössbauer Spectrometer, and MiniCorer required dedicated electronics boards and interfaces in the FIDO PEB.

[61] All the instruments can be run in laboratory settings with separate test setups. In this regard, however, the IPS's modular design is the most flexible. The IPS PC and electronics are all housed in a shielded, removable rack, and the IPS PC communicates with FIDO's computer via an internal Ethernet connection. A simple Internet protocol number change reconfigures the IPS for bench-top use. While some laboratory measurements, JPL Mars Yard, and field test calibration data were acquired with the IPS resident inside FIDO, most IPS characterization data were obtained with the IPS outside of the rover.

[62] The only instrument functions that were not fully integrated with FIDO hardware and software were the microscopic imager illumination ring and the IPS standby mode. The two LEDs of the microscopic imager illumina-

tion ring were turned on and off by the rover crew using a simple switch inside FIDO's electronics bay under its solar panel hardback. There is no technical reason not to fully integrate this switch and control it via the WITS software like the other instrument commands. This was a planned upgrade. Similarly, the IPS power management discussed earlier relied on field team activation of a stand-by mode and reactivation of the IPS PC for data acquisition.

[63] Certain instrument functions were disabled to improve instrument predictability and to better emulate their Martian analogues. For example, as discussed earlier, the Pancam automatic exposure was disabled to enable absolute radiometry with the LCTF filter set. For other tests the color information could be removed from the microscopic imager data delivered to the science team, making FIDO's data more qualitatively similar to Athena Payload Microscopic Imager data. Deployable instrument covers, while a possibility for Martian configurations, where dust is a concern, were not used for any of the FIDO instruments. Notwithstanding this exception and the others mentioned earlier, FIDO's integrated instrument suite provides a capable functional emulation of a mobile science platform for Mars exploration.

8.2. Instrument Suite Integrated Operations

[64] FIDO's science instrument suite was operated in field conditions in April 1999, October 1999, and May 2000. Acquired data are listed in Table 7. The April 1999 science team was at the Silver Lake site with FIDO [*Arvidson et al.*, 2000] and was able to directly observe its progress. Some operations were carried out "over the horizon" to begin training operations in unknown terrain. The October 1999 test was a short test at Silver Lake with field participation by some of the science team. The October 1999 test served as a test of WITS, rover, and instrument upgrades, like those that had been made to the IPS. The science team for the 2000 field test was "blind"; the team members were unaware of and unfamiliar with the actual location of the rover at Black Rock Summit, Nevada [*Arvidson et al.*, 2002].

[65] For all the tests, though most critically for the blind test in 2000, the science team's situational awareness of the rover in its environment was based on use of WITS. The team viewed image panoramas acquired by FIDO with this soft-

ware and designated targets within the spatially referenced data set. Later IPS or in situ instrument observations were tied to their targets for science evaluation. WITS' Internet-based client system allowed group collaboration by distributed users. WITS automated terrain traversability analysis and arm reachability analysis which the science team and rover engineers could include early in the planning process for target designation.

[66] FIDO operations were broken down into Mars-like cycles. Typically, one Mars day, or sol, of operations of the spacecraft which FIDO emulates begins with a wake-up sequence possibly followed by run-out commands from the previous day's command sequence followed by a morning communications link for data downlink and command uplink. The rover then executes its new sequence prior to an afternoon communications session for data downlink and then goes into an overnight low-activity "sleep" mode. The operations team on Earth will typically evaluate the sol's activities and generate the plan for the following sol during the Martian night. FIDO operations did not follow a strict one-to-one Earth-to-Mars correspondence. Instead, we compressed several single-sol operations cycles into an Earth day, bookkeeping the number of 'sols' required for execution of a given activity or scenario. This provides a metric for evaluating the effectiveness of the various operations scenarios.

[67] The science team's goal with its operations plan is to use FIDO's full instrument suite to develop a geologic understanding of a "landing site." Aspects of this process are described by *Arvidson et al.* [2002], *Jolliff et al.* [2002], and *Moersch et al.* [2002]. The planned science protocol of remote-sensing characterization of the site followed by in situ analysis of specific targets proved both appropriate and highly successful. Each field test began with a Navcam panorama for navigational planning and target designation with WITS and also with (April 1999 and May 2000) full 3-band Pancam stereo panoramas. Panorama acquisition could take more than one sol. Target designation was followed by roving toward the specified location. Further remote-sensing data from closer range were acquired prior to a final target approach phase. Once positioned, FIDO could deploy its arm or the drill. This typical sequence of events was repeated with more or less remote-sensing data acquisition as FIDO moved from one target location to the next.

8.3. Lessons Learned

[68] The lessons learned from the operational use of FIDO's integrated science instrument suite can be grouped into (1) science operations, (2) science analysis, and (3) instrument emulation fidelity.

8.3.1. Science Operations

[69] *Arvidson et al.* [2000, 2002] discuss the science operations lessons learned relating to how well various approaches to geoscientific hypothesis testing with FIDO worked at each of the landing sites. In general, the algorithm of remote sensing followed by targeted in situ sampling allowed the science team to construct an appropriate understanding of the sites. This was particularly true at Black Rock, Nevada, where the team was "blind." Much was also learned about the usefulness, limitations, and possible improvements to WITS and other software tools. In the time-compressed environment of FIDO operations, the science team wanted faster display of large Pancam panor-

amas, for instance, so that science decision making, and not software, was the rate-determining step. A second science operations lesson was that the science team's performance improved as their familiarity with the details of instrument operation improved. Some of the limitations of field use of the IPS were that it required (1) direct solar illumination of a target surface to provide a spectrum with good SNR and (2) produced better SNR spectra for higher-albedo targets. Once the team understood these points, their success rate with the IPS increased.

8.3.2. Science Analysis

[70] Closely related to the issue of software improvement for image display is the science analysis lesson that spectral analysis software and methods need to be paced to the command sequence development timeline. The IPS can serve to directly identify the presence or absence of certain minerals in the landscape [*Jolliff et al.*, 2002]. To use this information in a timely manner for science planning purposes, the quality of each raw spectrum needs to be assessed. Then IR reflectance spectra need to be generated, using calibration spectra. These need to be individually assessed by an analyst and the results shared with the planning team. Pancam provides the capability for an analogous remote target designation based on compositional analysis. However, Pancam image processing and operational calibration is more involved than for the IPS and was not carried out during the tests discussed here. Since the required calibrations of Pancam were performed, both in controlled laboratory situations and throughout operations using the calibration target on FIDO, subsequent analysis to demonstrate the capability could still be carried out.

8.3.3. Instrument Emulation Fidelity

[71] The FIDO science instrument suite was designed as an emulation of Mars mobile science platforms. Operational limitations are discussed in the earlier instrument sections. Some of the sometimes important differences between FIDO and Athena instruments had consequences for FIDO use and the lessons learned. To better emulate spacecraft instruments, we did implement the microscopic imager illuminator ring and IPS standby command functionality in WITS for the May 2000 field test. The command sequence sent to the field included, and in fact required, commands to activate the IPS and illuminator ring if their use was anticipated. However, command execution was still done by a human hand, without direct indication in the rover's telemetry that the action had occurred. In the case of poor data quality, from the IPS, for example, this potential failure mode was often considered, although the actual reason for low signal-to-noise IPS data was poor solar illumination, clouds, or a dark target rock in all but one case. These difficulties do not emulate Mars instrument operations; however, flexible IPS use within constraints provided important human and sequence planning lessons for achieving efficient use of a mobile science platform. Future science teams will need to be prepared to reacquire data from some targets if telemetry is lost or perhaps choose to either not move the rover or return to an important target later. The fact that the science teams did not choose to evaluate spectral information from Pancam also serves the lesson that some forms of scientific data may not be available within the planning cycle for daily rover operations and that a choice can be made to use other data types to plan tactical operations. Of course, the FIDO Pancam filters were chosen to emulate

the Athena Pancam, but with far fewer filters, that emulation is limited. In hindsight, for the quick turnaround operations planning it may have been better to design a three-band visible color camera so that a scene could be directly evaluated by a geologist with field experience. Some of the team's frustration at not being able to do this in the 1999 tests was the reason for finding a false-color combination that closely resembled true color (Figure 9).

9. Conclusion

[72] The FIDO science payload provides a field-deployable emulation of the Athena Science Payload for Mars rover missions and is used to test operations concepts for remote planetary geological investigations and, in particular, science operations scenarios for Mars. These primary payload requirements are fulfilled by the assembly of the entire suite of capable instruments into an integrated robotic tool for geoscientific enquiry.

[73] The selection and design of the FIDO Pancam, microscopic imager, IPS, and MiniCorer emulated the Athena instrument suite functionality. Thus the FIDO suite enabled emulation of Athena Science Payload operations, evaluation of mission scenarios, and enhanced training of scientists to support future operations on Mars.

[74] The usefulness of the FIDO instrument suite in meeting these objectives was greatly enhanced by the high degree of hardware and software integration of the suite with the FIDO rover. Software integration allowed the science team to seamlessly perform both robotic mobility and science observations. Hardware integration allowed the engineers to address issues inherent in the mobility system and science instruments sharing physical space and resources, resulting in design improvements for flight implementation.

[75] Calibration of the FIDO instruments has enabled FIDO to perform actual science, to better emulate Martian science operations, and to give the science team a preview of some of the data interpretation issues to be faced on Mars. Integration of calibration targets on board FIDO enabled ongoing evaluation of instrument performance over time.

[76] Finally, one of the most exciting aspects of the FIDO instruments is that they were designed and are utilized as a suite of instruments. They work together to achieve science goals of identifying scientific targets and analyzing them. The FIDO instrument suite working in conjunction with "blind" scientists controlling FIDO from their home institutions and in-field engineers providing ground truth enables evaluation of mission scenarios in terms of their effectiveness in achieving scenario objectives. Thus both the advantages and disadvantages of instrument configurations and mission scenarios can be identified and compared. The complexity encountered in the integration and calibration of FIDO's instrument suite is a precursor for future mobile scientific payloads to planetary surfaces. More than likely, both the scientists' and the engineers' experiences with FIDO's payload will provide useful inputs to future designs.

[77] **Acknowledgments.** The work described in this paper was principally performed at the Jet Propulsion Laboratory, a division of the California Institute of Technology under contract to NASA. Ray Arvidson and Nathaniel Snider were supported by the NASA Planetary Geology and Geophysics Program under Goddard Space Flight Center grant NAG5-7830. The FIDO instrument suite was supported by NASA's Mars Technology Program. Many people provided significant contributions to the FIDO instrument suite and

the preparation of this paper. In particular, we would like to thank Lee Magnone, Anthony Lai, Jeff Norris, Paul Backes, Brett Kennedy, Ashitey Trebi-Ollennu, Mike Garret, and Paul Schenker at JPL, Sudhir Trivedi, Zbigniew Kurbiel, and Igor Nazarov at Brimrose Corporation, and Stephanie Nelson and Bethany Ehlmann at Washington University in St. Louis.

References

- Arvidson, R. E., et al., Rocky 7 prototype Mars rover field geology experiments, *J. Geophys. Res.*, *103*, 22,671, 1998.
- Arvidson, R. E., S. S. Squyres, E. Baumgartner, L. Dorsky, and P. Schenker, Rover trials for Mars Sample Return Mission prove successful, *Eos Trans. AGU*, *81*, 65, 72, 2000.
- Arvidson, R. E., S. W. Squyres, E. T. Baumgartner, P. S. Schenker, C. S. Niebur, K. W. Larsen, F. P. Seelos IV, N. O. Snider, and B. L. Jolliff, FIDO prototype Mars rover field trials, Black Rock Summit, Nevada, as test of the ability of robotic mobility systems to conduct field science, *J. Geophys. Res.*, *107*, 10.1029/2000JE001464, 2002.
- Backes, P. G., and J. S. Norris, Automated rover sequence report generation, paper presented at IEEE Aerospace Conference, Inst. of Electr. and Electron. Eng., Big Sky, Mont., 2001.
- Backes, P. G., G. K. Tharp, and K. S. Tso, The Web Interface for Tele-science (WITS), paper presented at IEEE International Conference on Robotics and Automation, Inst. of Electr. and Electron. Eng., Albuquerque, N. M., 1997.
- Backes, P. G., K. S. Tso, J. S. Norris, G. K. Tharp, J. T. Slostad, R. G. Bonitz, and K. S. Ali, Internet-based operations for the Mars Polar Lander mission, paper presented at 2000 IEEE International Conference on Robotics and Automation, Inst. of Electr. and Electron. Eng., San Francisco, Calif., 2000.
- Bell, J. F., III, et al., Mineralogic and compositional properties of Martian soil and dust: Results from Mars Pathfinder, *J. Geophys. Res.*, *105*, 1721–1755, 2000a.
- Bell, J. F., III, K. E. Herkenhoff, M. Schwochert, R. V. Morris, R. Sullivan, and the Athena Science Team, The Athena Pancam and color microscopic imager (CMI), in *Workshop on Concepts and Approaches for Mars Exploration*, abstract 6104, Lunar and Planet. Inst., Houston, Tex., 2000b.
- Christensen, P. R., G. L. Mehall, N. Gorelick, S. Silverman, and the Athena Science Team, The Athena miniature thermal emission spectrometer (Mini-TES), in *Workshop on Concepts and Approaches for Mars Exploration*, abstract 6106, Lunar and Planet. Inst., Houston, Tex., 2000.
- Harris, S. E., and R. W. Wallace, Acousto-optic tunable filter, *J. Opt. Soc. Am.*, *59*, 744, 1969.
- Jolliff, B., A. Knoll, R. V. Morris, J. Moersch, H. McSween, M. Gilmore, R. E. Arvidson, R. Greeley, K. Herkenhoff, and S. Squyres, Remotely sensed geology from lander-based to orbital perspectives: Results of FIDO rover May 2000 field tests, *J. Geophys. Res.*, *107*, 10.1029/2000JE001470, 2002.
- Klingelhöfer, G., B. Fegley Jr., R. V. Morris, E. Kankleit, P. Held, E. Evlanov, and O. Priloutskii, Mineralogical analysis of Martian soil and rock by a miniaturized backscattering Mössbauer spectrometer, *Planet. Space Sci.*, *44*, 1277–1288, 1996.
- Moersch, J. E., B. L. Jolliff, H. Y. McSween, R. V. Morris, M. Gilmore, R. E. Arvidson, and S. W. Squyres, Synthesis of overhead and ground-based infrared spectroscopy at the 2000 FIDO Mars rover field test, *J. Geophys. Res.*, *107*, 10.1029/2001JE001524, 2002.
- Morris, R. V., and G. Klingelhöfer, Mössbauer mineralogy on Mars, in *Workshop on Early Mars*, abstract 3047, Lunar and Planet. Inst., Houston, Tex., 1997.
- Morris, R. V., et al., Mineralogy, composition, and alteration of Mars Pathfinder rocks and soils: Evidence from multispectral, elemental, and magnetic data on terrestrial analogue, SNC meteorite, and Pathfinder samples, *J. Geophys. Res.*, *105*, 1757–1818, 2000.
- Myrick, S. P., S. P. Gorevan, C. Batting, S. Stoescu, M. Maksymuk, K. R. Davis, M. A. Umy, and the Athena Science Team, The Athena miniature rock coring and rock core acquisition and transfer system (Mini-Corer), in *Workshop on Concepts and Approaches for Mars Exploration*, abstract 6105, Lunar and Planet. Inst., Houston, Tex., 2000.
- Schenker, P. S., et al., FIDO Rover and long-range autonomous Mars science, in *Intelligent Robots and Computer Vision XVIII: Algorithms, Techniques and Active Vision, Proc. SPIE Int. Soc. Opt. Eng.*, 3837, Boston, Mass., Sept. 1999.
- Schenker, P. S., T. L. Huntsberger, P. Pirjanian, and E. T. Baumgartner, Planetary rover developments supporting Mars science, sample return and future human-robotic colonization, paper presented at 10th IEEE International Conference on Advanced Robotics (ICAR 2001), Inst. of Electr. and Electron. Eng., Budapest, Hungary, 22–25 Aug. 2001.
- Smith, P. H., et al., The imager for Mars Pathfinder experiment, *J. Geophys. Res.*, *102*, 4003–4025, 1997.
- Squyres, S. W., and the Athena Science Team, The Athena Mars rover

investigation, in *Workshop on Concepts and Approaches for Mars Exploration*, abstract 6148, Lunar and Planet. Inst., Houston, Tex., 2000.

Tran, C. D., Acousto-optic devices: Optical elements for spectroscopy, *Anal. Chem.*, *64*, 971A–981A, 1992.

Wang, A., L. A. Haskin, B. Jolliff, T. Wdowiak, T. Agresti, A. L. Lane, and the Athena Science Team. The Athena Raman spectrometer, in *Workshop on Concepts and Approaches for Mars Exploration*, abstract 6030, Lunar and Planet. Inst., Houston, Tex., 2000.

R. E. Arvidson and N. O. Snider, Department of Earth and Planetary Sciences, Washington University, St. Louis, MO 63130, USA.

E. T. Baumgartner, G. H. Bearman, D. L. Blaney, D. I. Brown, B. P. Dolgin, L. I. Dorsky, A. F. C. Haldemann, T. L. Huntsberger, A. Ksendzov, J. C. Mahoney, M. J. McKelvey, B. E. Pavri, G. A. Post, and E. F. Tubbs, Jet Propulsion Laboratory, California Institute of Technology, 4800 Oak Grove Drive, Pasadena, CA 91109-8099, USA. (Albert.F.Haldemann@jpl.nasa.gov)

S. Gorevan, Honeybee Robotics Inc., New York, NY 10012, USA.

G. Klingelhöfer, B. Bernhardt, and R. Gellert, Institute for Inorganic and Analytical Chemistry, Johannes Gutenberg University Mainz, D-55099 Mainz, Germany.

S. W. Squyres, Center for Radiophysics and Space Research, Cornell University, Ithaca, NY 14853, USA.